Journal of Solid State Chemistry 208 (2013) 109–115

Contents lists available at ScienceDirect

Journal of Solid State Chemistry

journal homepage: www.elsevier.com/locate/jssc

Thermoelectric misfit-layered cobalt oxides with interlayers of hydroxide and peroxide species

Ta-Lei Chou [a], Jenni Lybeck [a], Ting-Shan Chan [b], Ying-Ya Hsu [c], Girish C. Tewari [a], Eeva-Leena Rautama [a], Hisao Yamauchi [a], Maarit Karppinen [a,*]

[a] Laboratory of Inorganic Chemistry, Department of Chemistry, Aalto University, FI-00076 Aalto, Finland
[b] National Synchrotron Radiation Research Center, Hsinchu 30076, Taiwan
[c] Program for Science and Technology of Accelerator Light Source, National Chiao Tung University, Hsinchu 30076, Taiwan

ARTICLE INFO

Article history:
Received 11 July 2013
Received in revised form
30 September 2013
Accepted 7 October 2013
Available online 16 October 2013

Keywords:
Misfit-layered cobalt oxide
Thermoelectric oxide
Low-temperature hydrothermal synthesis
Thermogravimetry
X-ray absorption spectroscopy

ABSTRACT

Among the thermoelectric misfit-layered cobalt oxides, $[M_mA_2O_{m+2}]_qCoO_2$, the parent $m=0$ phases exhibit divergent chemical features but are less understood than the more common $m>0$ members of the series. Here we synthesize Sr-for-Ca substituted $[(Ca_{1-x}Sr_x)_2(O,OH)_2]_qCoO_2$ zero phases up to $x=0.2$ through low-temperature hydrothermal conversion of precursor powders of the $m=1$ misfit system, $[Co(Ca_{1-x}Sr_x)_2O_3]_qCoO_2$. In the zero-phase $[(Ca_{1-x}Sr_x)_2(O,OH)_2]_qCoO_2$ system, as the Sr content x increases the lattice expands anisotropically along the c axis such that the ab-plane dimension and the misfit parameter q remain essentially constant. X-ray absorption spectroscopy data suggest the presence of peroxide-type oxygen species in the $(Ca_{1-x}Sr_x)_2(O,OH)_2$ rock-salt block and together with infrared spectroscopy, thermogravimetric and low-temperature resistivity and thermopower measurements evidence that the isovalent Sr-for-Ca substitution controls the balance between the peroxide and hydroxide species in the $(Ca_{1-x}Sr_x)_2(O,OH)_2$ block but leaves the valence of Co essentially intact in the CoO_2 block. The higher electrical conductivity of the Sr-substituted phases is explained as a consequence of increased carrier mobility.

© 2013 Elsevier Inc. All rights reserved.

1. Introduction

Various exciting physical properties such as high thermopower [1], giant magnetoresistance [2], superconductivity [3], and non-correlated metallic state [4,5] have been discovered since late 1990s for layered cobalt-oxide compounds based on the hexagonal CdI_2-type CoO_2 layer. In particular, the so-called misfit-layered cobalt oxides with a general formula of $[M_mA_2O_{m+2}]_qCoO_2$ (A=*e.g.* Ca, Sr, Ba; M=*e.g.* Co, Bi, Pb, Tl; m=0, 1 or 2) [6,7] are highly interesting from both scientific and technological points of view. The interest arises from the fact that they have been found to exhibit exceptionally high values of the thermoelectric figure-of-merit, Z ($\equiv S^2/\rho\kappa$) [8]. The high Z value requires the material to be simultaneously a good electrical conductor (with low resistivity, ρ) and a poor thermal conductor (with low thermal conductivity, κ), and to possess a large Seebeck coefficient (S).

It is their unique crystal structures that make it possible for the misfit-layered cobalt oxides to possess the required combination of properties being contradictory in conventional materials. The crystal structures consist of two types of layer-block: hexagonal CoO_2 and rock-salt-structured $M_mA_2O_{m+2}$, stacked incoherently to each other; the "misfit parameter" q ($\equiv b_H/b_{RS}$ with b_H and b_{RS} being the b lattice parameters of the two types of block along which the layers are by definition misfitting and to which the layer-stacking direction is perpendicular) is a measure of the mismatch between the two layer-blocks, a commensurate structure appearing only at q=0.50. Another important factor is the mixed-valence Co^{3+}/Co^{4+} state that provides pathways for carrier hopping and high thermopower as a result of the collective spin and orbital degeneracies [9]. Various chemical substitutions have been employed to control the magnitude of q and the valence state of cobalt. Basically, aliovalent substitutions that decrease the low-spin Co^{4+} content in the hexagonal CoO_2 layer would enhance the thermopower. This is not straightforward though, as factors like oxygen nonstoichiometry [10,11], carrier concentration and carrier mobility should be considered as well. Also, in a way parallel to artificial superlattices [12,13] the uniaxially-modulated misfit-layered structure as such presents weak correlation between the different layer-blocks, thus acting as a phonon scattering center to depress the thermal conductivity and increase the Z value.

The parent or "zero" (m=0) misfit-layered cobalt-oxide phases differ from the higher members of the $[M_mA_2O_{m+2}]_qCoO_2$ homologous series as they require synthesis conditions other than

* Correspondence to: Department of Chemistry, Aalto University, P.O. Box 16100, FI-00076 AALTO, Finland. Tel.: +358 50 384 1726; fax: +358 9 462 373.
E-mail address: maarit.karppinen@aalto.fi (M. Karppinen).

0022-4596/$ - see front matter © 2013 Elsevier Inc. All rights reserved.
http://dx.doi.org/10.1016/j.jssc.2013.10.012

ambient air to form [14–20]. The $m=0$ structure was first realized for $A=$Sr samples synthesized in a sealed quartz ampoule using SrO_2 and $SrCl_2\cdot 6H_2O$ as sources of excess oxygen and H_2O vapour, respectively [14,15], yielding samples with $q=0.50$, and later also through ultra-high-pressure synthesis [21] to obtain samples with $q\approx 0.53$ [16,17]. Partial substitution of Sr by Ca was achieved up to $y=0.2$ in the $[(Sr_{1-y}Ca_y)_2(O,OH)_2]_qCoO_2$ system, the samples being synthesized by the aforementioned closed-ampoule technique [15]. On the other hand, the non-doped zero phase with $A=$Ca was first obtained through ultra-high-pressure synthesis from CaO, CaO_2, $Ca(OH)_2$ and Co_3O_4 precursors. Actually, two polymorphs were reported: (1) monoclinic $[Ca_{1.7}(OH)_2]_{0.58}CoO_2$ being metallic with thermoelectric properties (*e.g.* $S_{300\ K}\approx 100\ \mu V/K$) typical for misfit-layered cobalt oxides, and (2) orthorhombic $[Ca_2(OH)_2]_{0.57}CoO_2$ being semiconducting with an extraordinarily high $S_{300\ K}\approx 330\ \mu V/K$ [18,19,22,23]. Later, Pei et al. [20] synthesized the monoclinic phase using a low-temperature hydrothermal technique where $Ca_2Co_2O_5$ was employed as a precursor. Here in this work we use – instead of $Ca_2Co_2O_5$ – the $m=1$ misfit-layered phase, $[CoCa_2O_3]_{0.62}CoO_2$, as a precursor. This allows us to extend the hydrothermal technique to the synthesis of Sr-for-Ca substituted $[(Ca_{1-x}Sr_x)_2(O,OH)_2]_qCoO_2$ samples up to $x=0.2$, and hence stabilize an important portion of the missing compositions in the $[(Ca,Sr)_2(O,OH)_2]_qCoO_2$ system, and in general shed light on the complex crystal structure-chemical state-physical property relations in the misfit-layered cobalt-oxide materials.

2. Experimental details

The $[Co(Ca_{1-x}Sr_x)_2O_3]_qCoO_2$ ($x=0$, 0.1, 0.2, 0.3 and 0.5) precursors were synthesized by a citrate-based sol–gel process. Stoichiometric amounts of $CaCO_3$, $SrCO_3$, $Co(NO_3)_2\cdot 6H_2O$ and anhydrous citric acid were dissolved in distilled water with stirring followed by mild heating at 100 °C until the gel formed. After drying at 200 °C overnight, the ash was ground and calcined at 600 °C to remove the organic residues. Finally, the powders were pressed into pellets and sintered at 900 °C for 24 h to reach decent crystallinity.

In the hydrothermal process, appropriate amounts of the $[Co(Ca_{1-x}Sr_x)_2O_3]_qCoO_2$ precursor (50 mg) and the mineralizing agent $NaOH_{(aq)}$ solution (30 ml) were mixed and sealed in a Teflon-line vessel (Parr 4744) such that the filling rate was 66.7%. The hydrothermal synthesis was carried out at 220 °C for 48 h, after which the vessel was cooled down to room temperature, the product was washed with distilled water repeatedly, and finally filtered and dried in an oven at 100 °C overnight. The actual Sr-to-Ca ratio in the samples was confirmed by inductively coupled plasma atomic emission spectrometry (ICP-AES, Perkin Elmer 7100 DV). For the ICP-AES analyses the sample powders were digested by *aqua regia* in closed teflon vessels in a microwave oven (Milestone, ETHOS 1200) at 200 °C for 50 min.

All the hydrothermal synthesis products were first checked for the phase purity by our in-house X-ray powder diffractometer (XRD; PanAnalytical X'Pert PRO with Cu-$K\alpha_1$ source). The crystal structures were analyzed for the essentially single-phase samples using synchrotron X-ray powder diffraction ($E=16$ keV, $\lambda=0.7749$ Å) data collected at room temperature at the BL 01C2 end station in National Synchrotron Radiation Research Center (NSRRC), Taiwan. Lattice parameters were obtained from Le Bail fittings using the FullProf package and space group *C2/m* both for the hexagonal and rock-salt sub-blocks.

Thermal properties of the samples were investigated with thermogravimetric (TG; PerkinElmer Pyris 1) measurements carried out in both 80% N_2–20% O_2 and 5% H_2–95% Ar gas flows with a heating rate of 5 °C /min up to 900 °C . A constant sample mass of ~20 mg was used for each measurement.

The electronic states of cobalt and oxygen were investigated through room-temperature X-ray absorption spectroscopy (XAS) measurements carried out for the $x=0$ and 0.2 samples (*plus* $LaCoO_3$ and $[CoCa_2O_3]_{0.62}CoO_2$ as references) at *O–K* and Co-$L_{2,3}$ edges at the end station BL 20A in NSRRC (under ultra-high vacuum in electron-yield mode) and at Co-*K* edge at the BL 01C1 end station (in transmission mode). For comparison we normalized the post-edge region of all calibrated spectra to unity.

Fourier transform infrared (FTIR, Nicolet Magna 750) spectrometry was used to investigate the hydroxide and peroxide groups in the $x=0$, 0.1 and 0.2 samples and also in the two misfit cobalt oxides, $[CoCa_2O_3]_{0.62}CoO_2$ and $[Sr_2(O,OH)_2]_{0.52}CoO_2$, for comparison. All the samples were first left in an oven at 120 °C overnight to remove adsorbed humidity then thoroughly mixed with KBr and pressed into dense pellets. Throughout the measurement the chamber was purged with dried air.

Temperature dependences of electrical resistivity (ρ) and Seebeck coefficient (S) were examined individually by using the four-probe technique and steady-state method, respectively, from room temperature down to 5 K in a liquid-He tank. For these measurements the samples were pressed into thin rectangular plates and heated at 275 °C for 72 h.

3. Results and discussion

In their hydrothermal synthesis of monoclinic $[Ca_{1.7}(OH)_2]_{0.58}CoO_2$, Pei et al. [20] used "$Ca_2Co_2O_5$" as a precursor. Previous works regarding the $Ca_2Co_2O_5$ phase (consisting of rows of oxygen and oxygen vacancies alternating along *c* axis) are however somewhat controversial [20,24,25]. In the present work despite of our best efforts, there was always CaO residue in the product when we aimed at stoichiometric $Ca_2Co_2O_5$, and the rest part of the XRD pattern highly resembled that of the misfit-layered $[CoCa_2O_3]_{0.62}CoO_2$ compound. We therefore decided to utilize $[CoCa_2O_3]_{0.62}CoO_2$ and its Sr-substituted derivatives as precursors in the present work. The phase diagram of the quaternary Ca–Sr–Co–O system has been systematically studied by several groups. In misfit-layered $[Co(Ca_{1-x}Sr_x)_2O_3]_qCoO_2$, the solubility limit of Sr at the Ca site is around $x=0.2$. Beyond this, $Sr_6Co_5O_{15}$ that consists of one-dimensional chains of face-shared CoO_6 octahedra appears as a second phase [26–28].

Then, when optimizing the hydrothermal synthesis process, we noticed that for the non-doped $[Ca_z(OH)_2]_qCoO_2$, 4 M $NaOH_{(aq)}$ solution as the mineralizing agent worked well, while higher concentrations of $NaOH_{(aq)}$ up to 9 M were needed for the Sr-for-Ca substituted samples. Single-phase misfit-layered $[(Ca_{1-x}Sr_x)_z(O,OH)_2]_qCoO_2$ products of the zero ($m=0$) structure were obtained up to $x=0.2$, *i.e.* as long as the $[Co(Ca_{1-x}Sr_x)_2O_3]_qCoO_2$ precursor was of single phase. Once impurities appeared in the precursor (for $x>0.2$), even a highly concentrated $NaOH_{(aq)}$ solution did not help to remove them from the final synthesis product. Fig. 1 displays the synchrotron powder XRD patterns for all our hydrothermally-synthesized $[(Ca_{1-x}Sr_x)_z(O,OH)_2]_qCoO_2$ samples. From ICP-AES analysis we could confirm that the actual Sr-to-Ca ratios in the single-phase Sr-substituted samples were very close to the aimed values: 10.4 mol-% for $x=0.1$ and 20.9 mol-% for $x=0.2$.

Lattice parameters a, b_H, b_{RS}, c and β, and the misfit parameter q, determined from the synchrotron X-ray diffraction data for the $[(Ca_{1-x}Sr_x)_z(O,OH)_2]_qCoO_2$ samples with $x=0$, 0.1, 0.2 and 0.3, are given in Table 1. Despite the presence of small amounts of impurities in the $x=0.3$ sample, the $[(Ca_{1-x}Sr_x)_z(O,OH)_2]_qCoO_2$ lattice expands with x up to ~0.3. From Table 1, it is noteworthy that the lattice expansion in the *ab* plane, compared to that along the *c* axis, is less evident. Also, the misfit parameter remains nearly

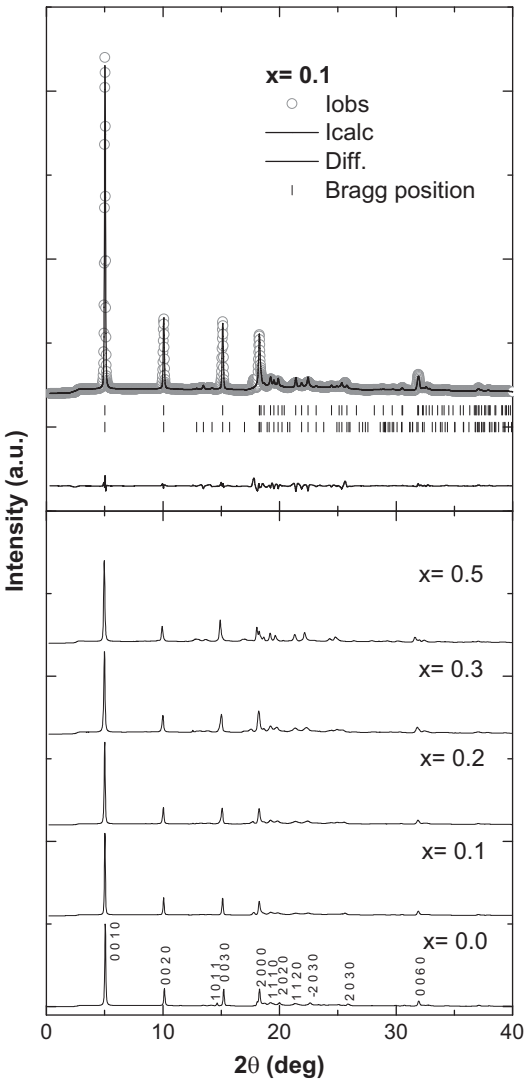

Fig. 1. Synchrotron X-ray powder diffraction patterns recorded for the hydrothermally-synthesized $[(Ca_{1-x}Sr_x)_zO,OH)_2]_qCoO_2$ samples ($x=0$, 0.1, 0.2, 0.3 and 0.5) using monochromatic source (E=16 keV, $\lambda=$ 0.7749 Å). The sample are essentially single-phase up to $x=0.2$. The upper panel presents the Le Bail fitting result for the $x=0.1$ sample.

Table 1
Lattice parameters from Le Bail fitting for the Sr-substituted $[(Ca_{1-x}Sr_x)_z(O,OH)_2]_qCoO_2$ samples. The space group used for the fittings is *C2/m*.

x	a	b_H	b_{RS}	c	β	q
0.0	4.89(4)	2.81(8)	4.87(2)	8.80(9)	95.7(2)	0.578
0.1	4.84(4)	2.82(6)	4.88(2)	8.89(8)	96.4(2)	0.579
0.2	4.85(5)	2.83(4)	4.88(6)	8.94(8)	96.4(3)	0.579
0.3	4.93(1)	2.82(4)	4.87(5)	9.00(7)	96.7(2)	0.579

constant at $q=0.58$. For the $x=0$ sample, the parameters obtained here are essentially identical to those previously reported for monoclinic $[Ca_{1.7}(OH)_2]_{0.58}CoO_2$ [29]. Hence we assume that at least for our $x=0$ sample, $z\approx 1.7$.

Thermal stability of the $[(Ca_{1-x}Sr_x)_zO,OH)_2]_{0.58}CoO_2$ ($x=0$, 0.1 and 0.2) phases was investigated by TG measurements in a synthetic air flow (Fig. 2). For the non-doped ($x=0$) sample, XRD data indicated that the product beyond 600 °C would be a mixture of $[CoCa_2O_3]_{0.62}CoO_2$ and a trace amount of CaO, implying that there is a complicated reconstruction process transforming the $Ca_z(O,OH)_2$ double-interlayers of the zero phase into CaO–CoO–CaO

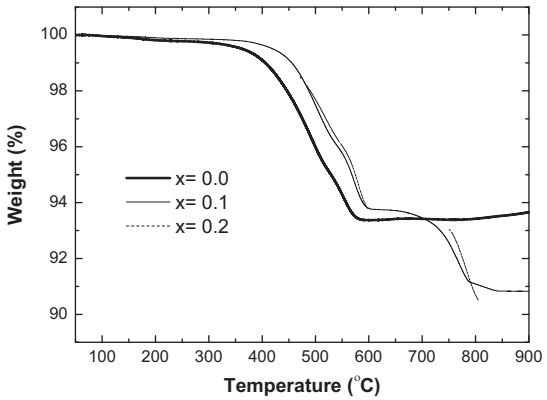

Fig. 2. TG curves for the $x=0$, 0.1 and 0.2 samples of $[(Ca_{1-x}Sr_x)_zO,OH)_2]_{0.58}CoO_2$ recorded upon heating in 80% N_2–20% O_2 gas flow at a heating rate of 5 °C/min^{-1}.

triple-layers ($m=1$) above a certain critical temperature. *In-situ* high-temperature XRD measurements would be needed to elucidate the entire story of this. On the other hand, for the Sr-substituted samples with $x=0.1$ and 0.2 the phase-decomposition occurs in air in two clearly separated steps, being completed only around 900 °C with a mixture of $[Co(Ca,Sr)_2O_3]_qCoO_2$ and $(Sr,Ca)CoO_{2.5+\delta}$ according to *ex-situ* XRD analysis.

Earlier we reported that not only for the purely Ca-based $[Ca_z(O,OH)_2]_qCoO_2$ zero misfit phase, but also for the Sr-rich phases $[(Sr_{1-y}Ca_y)_zO,OH)_2]_qCoO_2$ ($0\le y\le 0.2$) at least part of the oxide ions are replaced by OH^- groups in the rock–salt block [15,17]. To confirm this quantitatively for the present hydrothermally-synthesized Ca-rich phases $[(Ca_{1-x}Sr_x)_zO,OH)_2]_{0.58}CoO_2$ we carried out TG measurements in a reductive H_2–Ar atmosphere. From the curves presented for the $x=0$, 0.1 and 0.2 samples in Fig. 3a, it is seen that the weight losses are essentially larger than those measured in the N_2–O_2 gas flow; moreover the weight losses start at a lower temperature in H_2–Ar than in N_2–O_2. X-ray powder diffraction patterns for the products after the TG runs reveal that this is also the temperature range where the misfit-layered structure starts to collapse. In line with Ref. 30, we assign the low-temperature two-step weight losses in the temperature range of 270–420 °C to the hydroxide species extracted from the $[(Ca_{1-x}Sr_x)_{0.58}(O,OH)_2]_qCoO_2$ structure. Note that this temperature range is considerably higher than the temperatures where water molecules typically leave oxide networks. From 420 °C onwards the weight losses can be ascribed to the loss of oxygen. As shown in Fig. 3b, the contents of hydroxide and oxygen species go in an opposite trend with increasing Sr content x. Apparently Sr substitution in the $(Ca_{1-x}Sr_x)_zO,OH)_2$ rock-salt block leads to a reduced hydroxide-ion content and an increased oxygen content.

Next we turn our attention to the Co-*K* XAS data which could tell us the chemical state and local environment surrounding the Co atom in the hexagonal CoO_2 layer. Normalized spectra for our $x=0$ and 0.2 samples of $[(Ca_{1-x}Sr_x)_zO,OH)_2]_{0.58}CoO_2$ are presented in Fig. 4 together with spectra for the Co^{3+} compound $LaCoO_3$ and the misfit-layered $[CoCa_2O_3]_{0.62}CoO_2$ phase for comparison. The pre-edge peaks, denoted as A in Fig. 4, result from the Co 1*s* to 3*d* transition which turns allowed owing to the hybridization with *O* 2*p* states. In perovskite $LaCoO_3$, the CoO_6 octahedra are corner-shared and the observed doublet peaks can be assigned to the t_{2g} (7710.0 eV) and e_g (7712.3 eV) states [17,31]. In the spectra of misfit-layered cobalt oxides we only see a single peak in the pre-edge region A due to the modification of ligand field in the hexagonal CoO_2 layer of edge-shared CoO_6 octahedra. The intense white line marked as B in Fig. 4 originates from excitations from 1*s* to unoccupied 4*p* states and variations in this region reveal information of the valence state of cobalt, as well as bond

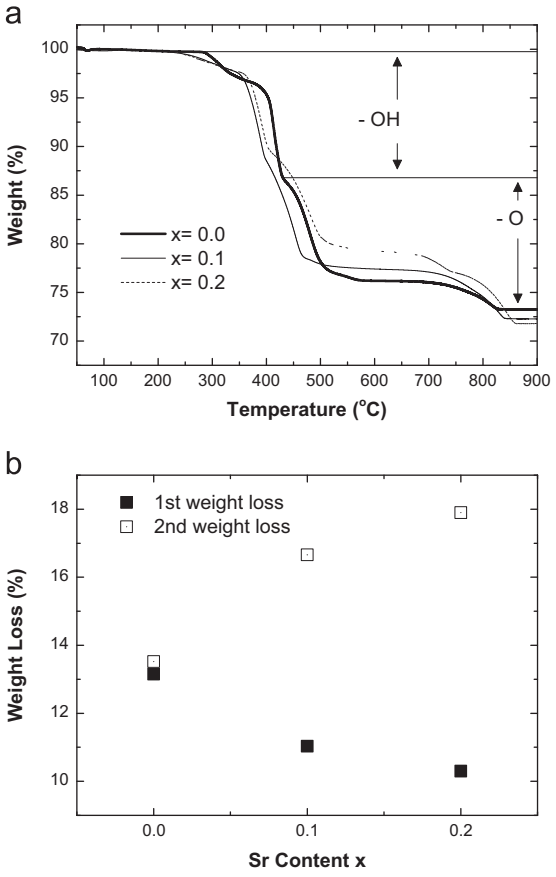

Fig. 3. (a) TG curves for the $x=0$, 0.1 and 0.2 samples of $[(Ca_{1-x}Sr_x)_z(O,OH)_2]_{0.58}CoO_2$ recorded upon heating in 5% H_2-95% Ar gas flow at a heating rate of 5 °C /min, and (b) the calculated weight losses for the same samples by 900 °C.

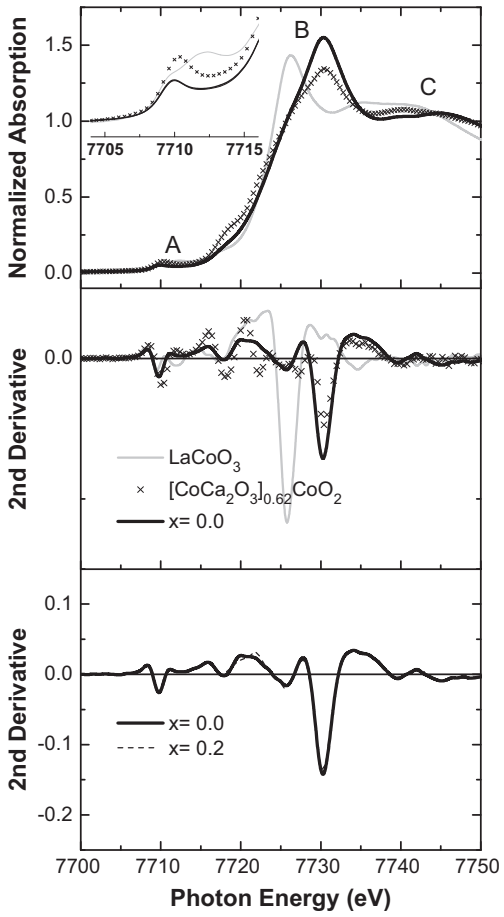

Fig. 4. Co-*K* XANES spectra for $LaCoO_3$ (grey line), $[Ca_2CoO_3]_{0.62}CoO_2$ (cross) and the $[(Ca_{1-x}Sr_x)_z(O,OH)_2]_{0.58}CoO_2$ samples of $x=0$ (thick solid line) and $x=0.2$ (dashed line). The corresponding secondary derivatives are plotted in the lower panels.

distances and the degree of ionic character between cobalt and its neighboring atoms [32]. Contrary to the trivalent-cobalt compound $LaCoO_3$, all the three misfit-layered phases show mixing components in the second derivatives of the spectra in region B. For $[CoCa_2O_3]_{0.62}CoO_2$ the broad second derivative of the white line in between 7720 and 7735 eV, which also reflects to the multiple scattering resonances in region C, can be explained by cobalt atoms distributed in two different sub-blocks. For our two $[(Ca_{1-x}Sr_x)_z(O,OH)_2]_{0.58}CoO_2$ samples, the spectra clearly present contributions from both trivalent and tetravalent cobalt around 7725 and 7730 eV, respectively. Somewhat surprisingly, no discernible spectral modifications are seen for the $x=0.2$ sample compared to the $x=0$ case. There are no obvious spectral modifications at the Co-$L_{2,3}$ absorption edge either due to the Sr-for-Ca substitution, see Fig. 5a. For the three $[(Ca_{1-x}Sr_x)_z(O,OH)_2]_qCoO_2$ phases, $x=0$, 0.2 and 1.0 (= $[Sr_2(O,OH)_2]_{0.52}CoO_2$[17]), the normalized spectra (Fig. 5a) superimpose on top of each other perfectly. The value of 0.67 obtained here for the so-called branching ratio [33] means that all the present phases have a low-spin state for cobalt. Looking back to the TG data, it thus seems that the decreasing OH- content and increasing oxygen content in the $(Ca_{1-x}Sr_x)_z(O,OH)_2$ rock–salt block with increasing Sr content x have no major effects on the state of cobalt in the CoO_2 layer. A plausible explanation for this may be revealed from the O–*K* edge XAS data, as described in the following.

At the O–*K* edge, the features existing in the 525–535 eV energy range originate from hybridizations between the Co 3*d* and O 2*p* orbitals, while the broad bumps centered at 538 and 542 eV are from alkaline-earth *d* and Co 4*sp* states, respectively (Fig. 5b). Compared to the triplet 3*d* states (α: Co^{4+} with a_{1g} symmetry; β: Co^{4+} with e_g symmetry; γ: Co^{3+} with e_g symmetry) in $[CoCa_2O_3]_{0.62}CoO_2$, the α and β components in the present two $[(Ca_{1-x}Sr_x)_z(O,OH)_2]_{0.58}CoO_2$ ($x=0$ and 0.2) samples are broader and not well split. Secondly, when we fit the pre-edge peaks with three Gaussian components, it is found that the 20% Sr substitution in $[(Ca_{1-x}Sr_x)_z(O,OH)_2]_{0.58}CoO_2$ results in only ~2% spectral weight transfer from α and β to γ, which is in accordance with the negligible modifications seen at the Co-$L_{2,3}$ edge. Interestingly, at the higher energy around 533.8 eV the present $[(Ca_{1-x}Sr_x)_z(O,OH)_2]_{0.58}CoO_2$ samples possess an extra peak, which has been interpreted as an indication of anionic dioxygen species in different solid systems [34–38]. We moreover confirmed that the peak was seen also in spectra recorded in the bulk-sensitive total fluorescence yield mode (not shown here). Echoing to the results from our TG and Co-*K*- and –$L_{2,3}$ edge XAS analyses, it seems that the anionic peroxide-like species might play the role of counterbalancing the effects of decreasing OH- content in the $(Ca_{1-x}Sr_x)_z(O,OH)_2$ block with increasing Sr content x such that the valence state of cobalt may remain essentially the same in the CoO_2 layer. In other words, the isovalent Sr-for-Ca substitution apparently controls the balance between hydroxide and peroxide species in the $(Ca_{1-x}Sr_x)_z(O,OH)_2$ block leaving the CoO_2 layer essentially intact (regarding the valence state, spin state and coordination sphere of cobalt).

To acquire further evidence of the presence of peroxide species in our $[(Ca_{1-x}Sr_x)_z(O,OH)_2]_{0.58}CoO_2$ samples FTIR spectroscopy was applied to investigate the vibration modes in the samples. Spectra for two other misfit-layered cobalt oxides, *i.e.*

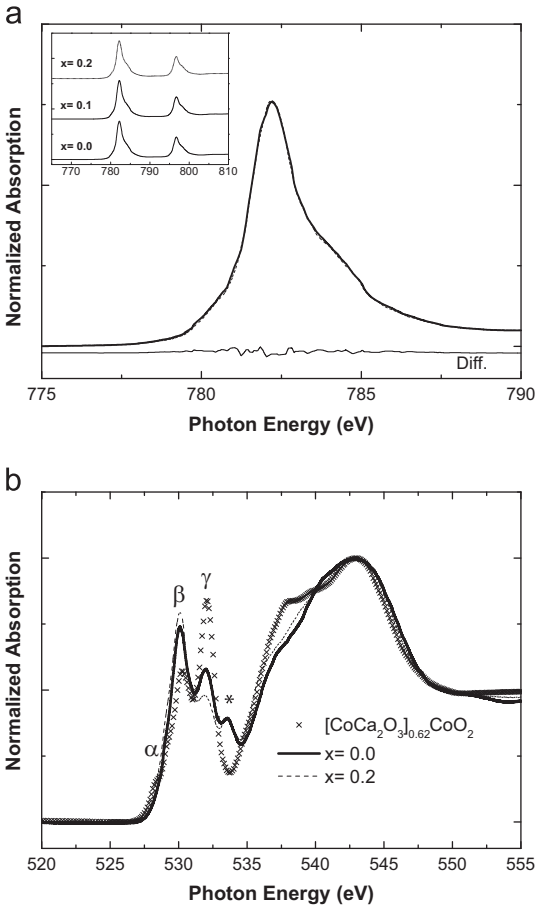

Fig. 5. XAS spectra at (a) Co-$L_{2,3}$ and (b) O–K edges for $[CoCa_2O_3]_{0.62}CoO_2$ (cross) and the $[(Ca_{1-x}Sr_x)_z(O,OH)_2]_{0.58}CoO_2$ samples of $x=0$ (thick solid line) and $x=0.2$ (dashed line). After energy calibration all the spectra were normalized to their maximal intensities. The asterisk in (b) indicates the peroxide group in the $[(Ca_{1-x}Sr_x)_z(O,OH)_2]_{0.58}CoO_2$ samples.

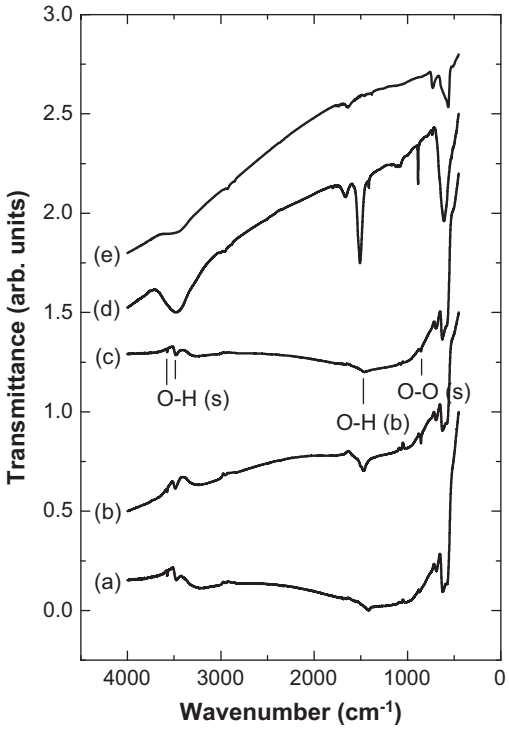

Fig. 6. FTIR spectra for various misfit-layered cobalt oxides: (a) $x=0$, (b) $x=0.1$, and (c) $x=0.2$ samples of the present $[(Ca_{1-x}Sr_x)_z(O,OH)_2]_{0.58}CoO_2$ system, and (d) $[Sr_2(O,OH)_2]_{0.52}CoO_2$ and (e) $[CoCa_2O_3]_{0.62}CoO_2$ for comparison.

Table 2
Positions (cm^{-1}) of FTIR spectral features (related to O–O stretching, O–H bending and O–H stretching) seen for the Sr-substituted $[(Ca_{1-x}Sr_x)_z(O,OH)_2]_qCoO_2$ samples and also for two other misfit-layered cobalt oxide phases for comparison.

Compounds	O–O stretching	O–H bending	O–H stretching	
$x=0.0$	863.6	1414.6	3475.2	3575.4
$x=0.1$	856.3	1419.5	3487.7	3575.4
$x=0.2$	855.3	1461.8	3479.9	3575.4
$[Sr_2(O,OH)_2]_{0.52}CoO_2$	856.3	1479.2	3448.2	
$[CoCa_2O_3]_{0.62}CoO_2$	No peak	No peak	No peak	No peak

$[CoCa_2O_3]_{0.62}CoO_2$ and $[Sr_2(O,OH)_2]_{0.52}CoO_2$, were recorded for comparison, see Fig. 6 and Table 2. First of all, the region below 1000 cm^{-1} is generally related to the vibrations of ions in the lattice [39]. The bands at around 600 and 700 cm^{-1} are respectively coming from the Co–O and (Ca,Sr)–(O,OH) vibrations. At higher wavenumbers, the peaks at around 850 cm^{-1}, although not that evident in the $x=0$ sample, can be assigned as the stretching mode of the dioxygen O–O group. The peaks at around 1480 cm^{-1} can be attributed to the asymmetrical bending mode of the O–H group. Compared to the regular value ~1600 cm^{-1} for H–O–H bending mode in $H_2O_{(l)}$, the red-shift could be most likely due to the strong interaction between the alkaline earths and the hydroxyl group. Finally, the features nearby 3500 cm^{-1} are widely known as the stretching modes of O–H group; note that since there is no peak seen around 1600 cm^{-1} we may conclude that the features related to O–H group here do not originate from adsorbed humidity.

Finally we investigated the electronic transport properties of the $[(Ca_{1-x}Sr_x)_z(O,OH)_2]_{0.58}CoO_2$ samples at low temperatures. As displayed in Fig. 7, the temperature dependences of both S and ρ for the non-doped $x=0$ phase are highly consistent with previous literature data [19,22,23]. The upturn in ρ below 10 K is commonly seen in misfit-layered cobalt oxides; yet the origin is unclear. With increasing Sr-for-Ca substitution level, resistivity goes decreasing more steeply as temperature reduces, meaning that the phase turns more metallic. Meanwhile, the low-temperature upturn diminishes. Instead of changes in carrier concentration (n), the marked change in the temperature dependence of this system would predominantly originate from changes in the carrier mobility (μ), which strongly depends on the defect content and the extent of order/disorder. Regarding their Seebeck coefficients, just like all known misfit-layered cobalt oxides the present $[(Ca_{1-x}Sr_x)_z(O,OH)_2]_{0.58}CoO_2$ phases have positive S values, meaning that holes are the predominant carriers. At 300 K the non-doped $x=0$ phase exhibits a decent value of S_{300K} ~115 μV/K like most high-performance thermoelectric misfit-layered cobalt oxides and drops abruptly nearby 150 K. For the Sr-substituted phases $S_{300\,K}$ drops to ~80 μV/K for $x=0.1$ and ~70 μV/K for $x=0.2$. Overall the temperature dependencies of transport properties for the present $[(Ca_{1-x}Sr_x)_z(O,OH)_2]_{0.58}CoO_2$ samples are quite similar. For the $x=0$ phase we find that the ρ–T curve in the temperature range 6.5–100 K can be fitted to the Efros-Shklovskii variable range hopping (ES-VRH) formula [40] (Fig. 8a):

$$\rho = \rho_0 exp(T_0/)T^{1/2}$$

where ρ_0 and T_0 are constants. The value of $T_0=12.2$ K as calculated from the linear region and the activation energy for conduction $E_\sigma=1.03$ meV suggests that the non-doped phase is nearly metallic. The activation energy for carrier generation E_S, on

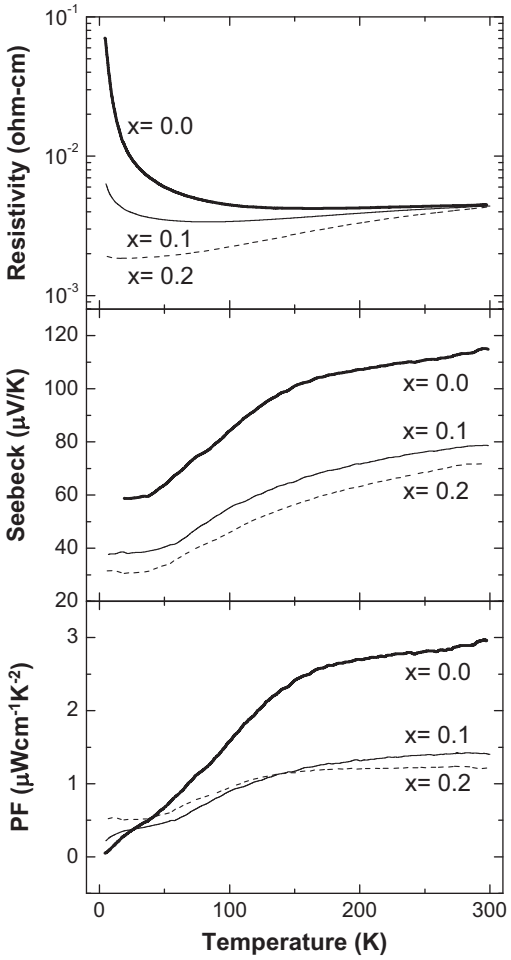

Fig. 7. Temperature-dependence of electrical resistivity, Seebeck coefficient, and power factor for the $[(Ca_{1-x}Sr_x)_z(O,OH)_2]_{0.58}CoO_2$ samples of $x=0$ (thick solid line), 0.1 (thin solid line) and 0.2 (dashed line) from room temperature down to 5 K.

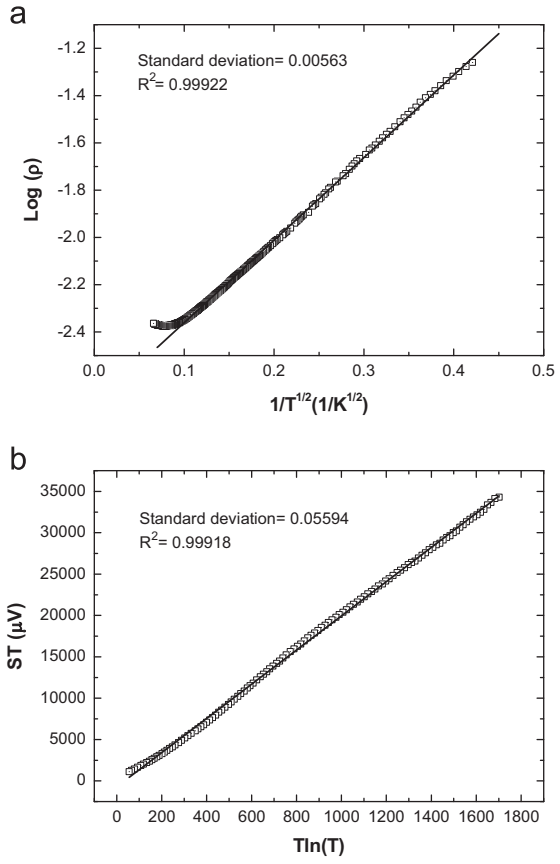

Fig. 8. Fitting results of the linear regions in (a) log(ρ) versus $1/T^{1/2}$ and (b) ST versus Tln(T) curves for the $x=0$ $[(Ca_{1-x}Sr_x)_z(O,OH)_2]_{0.58}CoO_2$ sample.

the other hand, can be obtained by fitting the linear region after re-plotting the curves according to the formula [41] (Fig. 8b):

$$ST = B \cdot T \ln T + C.$$

where B and C are constants. The value of E_S calculated from the interception C is 0.72 meV. The difference between E_σ and E_S implies that the carrier mobility is thermally activated. Finally, given that the power factor can be obtained by multiplying electrical conductivity σ and square of Seebeck coefficient S^2, we expect the maximal values of these specimens to exist above room temperature.

In Fig. 9 we plot the lattice parameters, misfit factors and $S_{300\ K}$ values for selected zero misfit-layered cobalt-oxide phases for comparison. Disregarding the missing members, we find feeble continuity within the entire $[(Ca_{1-x}Sr_x)_z(O,OH)_2]_qCoO_2$ system. While Sr gradually substitutes Ca, we find ~2% and ~3.3% expansion along a and c axes, respectively, as x increases from 0 to 1; a rather large ~12.5% lattice modification takes place along the b axis. But as mentioned earlier, among the Ca-rich phases the change along the c axis is more prominent. Concerning the misfit parameter q, overall the Ca-rich phases display higher values. Seebeck coefficients of these compounds obviously are poorly dependent on the Ca/Sr content. According to the discussion above, S is strongly related to the effective mass (m*) and carrier character. For further detailed discussions, in addition to measurements of carrier concentration and mobility we also have to refine the structures and precisely determine the chemical compositions, particularly the concentrations of Ca/Sr vacancies, in these phases.

4. Conclusion

The present work aimed at deeper understanding of the parent or so-called zero misfit-layered cobalt oxide phases that are promising candidates for future thermoelectric applications. The zero phases are structurally simpler yet chemically more complex than the higher members of the $[M_mA_2O_{m+2}]_qCoO_2$ misfit oxide family. In this work we were successful in realizing Sr-for-Ca substituted phases up to $x=0.2$ in the $[(Ca_{1-x}Sr_x)_z(O,OH)_2]_qCoO_2$ zero system through a hydrothermal synthesis process employing single-phase $[Co(Ca_{1-x}Sr_x)_2O_3]_qCoO_2$ powders of the $m=1$ misfit structure as precursors. The obtained zero-phase structure is thermally of somewhat limited stability, transforming back to the $m=1$ structure upon heating in air beyond ~500 °C .

Through structural, chemical and physical property characterization of the newly realized $[(Ca_{1-x}Sr_x)_z(O,OH)_2]_qCoO_2$ phases, we could learn that when the content of Sr increases, lattice expands mainly along the c axis, while the ab-plane dimension and the misfit parameter q remain essentially constant. From O–K edge X-ray absorption spectroscopy data an indication of the presence of peroxide-type oxygen species in the $(Ca_{1-x}Sr_x)_z(O,OH)_2$ rock-salt block was found for the first time; the presence of hydroxide species in the same block was revealed from thermogravimetric measurements. X-ray absorption spectra at Co-K and -L edges together with thermogravimetric and low-temperature transport-property measurements evidenced that the isovalent Sr-for-Ca substitution may affect the balance between the peroxide and hydroxide species in the $(Ca_{1-x}Sr_x)_z(O,OH)_2$ block but leaves the

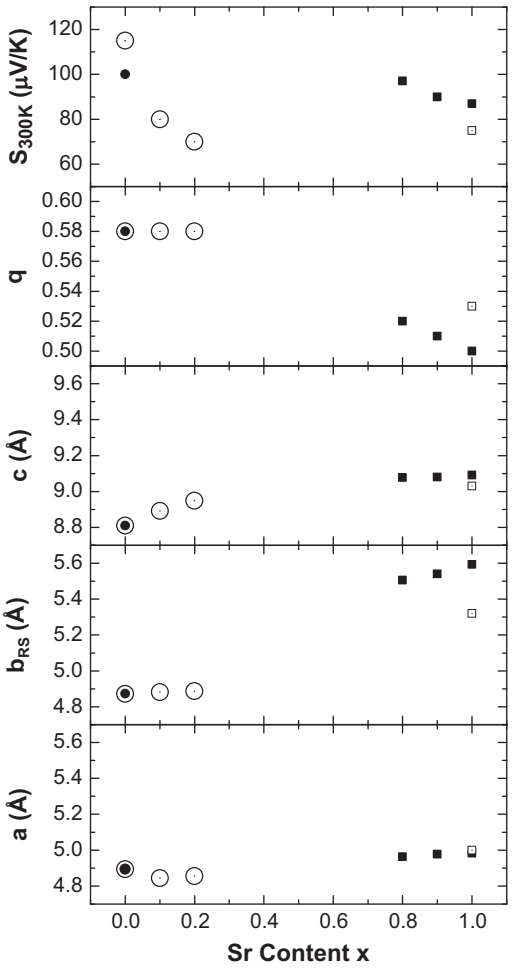

Fig. 9. A montage of lattice parameters, misfit parameters and the corresponding Seebeck coefficients at 300 K as a function of Sr content from selected double-interlayered misfit cobalt oxides. Filled square: Yamauchi et al. (15); unfilled square: Ishiwata et al. (16); filled circle: Shizuya et al. (23); unfilled circle: this work.

valence of Co essentially intact in the CoO_2 block. The higher electrical conductivity of the Sr-for-Ca substituted samples was attributed to the increased carrier mobility instead of the carrier concentration.

Acknowledgments

The present work was supported by Academy of Finland (No. 255562) and Tekes (No. 1726/31/07). The authors would like to thank the staff in NSRRC for their technical support in experimental setup and measurements.

References

[1] I. Terasaki, Y. Sasago, K. Uchinokura, Phys. Rev. B: Condens. Matter 56 (1997) 12685–12687.
[2] A.C. Masset, C. Michel, A. Maignan, M. Hervieu, O. Toulemonde, F. Studer, B. Raveau, J. Hejtmanek, Phys. Rev. B: Condens. Matter 62 (2000) 166–175.
[3] K. Takada, H. Sakurai, E. Takayama-Muromachi, F. Izumi, R.A. Dilanian, T. Sasaki, Nature 422 (2003) 53–55.
[4] T. Motohashi, Y. Katsumata, T. Ono, R. Kanno, M. Karppinen, H. Yamauchi, Chem. Mater. 19 (2007) 5063–5066.
[5] T. Motohashi, T. Ono, Y. Sugimoto, Y. Masubuchi, S. Kikkawa, R. Kanno, M. Karppinen, H. Yamauchi, Phys. Rev. B: Condens. Matter 80 (2009) 165114.
[6] P. Boullay, B. Domenges, M. Hervieu, D. Groult, B. Raveau, Chem. Mater. 8 (1996) 1482–1489.
[7] P. Boullay, R. Seshadri, F. Studer, M. Hervieu, D. Groult, B. Raveau, Chem. Mater. 10 (1998) 92–102.
[8] D.M. Rowe (Ed.), CRC Handbook of & Thermoelectrics: Macro to Nano, CRC, Boca Raton, 2005.
[9] W. Koshibae, K. Tsutsui, S. Maekawa, Phys. Rev. B: Condens. Matter 62 (2000) 6869–6872.
[10] M. Karppinen, H. Fjellvåg, T. Konno, Y. Morita, T. Motohashi, H. Yamauchi, Chem. Mater. 16 (2004) 2790–2793.
[11] Y. Morita, J. Poulsen, K. Sakai, T. Motohashi, T. Fujii, I. Terasaki, H. Yamauchi, M. Karppinen, J. Solid State Chem. 177 (2004) 3150–3156.
[12] L.D. Hicks, M.S. Dresselhaus, Phys. Rev. B: Condens. Matter 47 (1993) 12727–12731.
[13] R. Venkatasubramanian, E. Siivola, T. Colpitts, B. O'Quinn, Nature 413 (2001) 597–602.
[14] H. Yamauchi, K. Sakai, T. Nagai, Y. Matsui, M. Karppinen, Chem. Mater. 18 (2006) 155–158.
[15] H. Yamauchi, L. Karvonen, T. Egashira, Y. Tanaka, M. Karppinen, J. Solid State Chem. 184 (2011) 64–69.
[16] S. Ishiwata, I. Terasaki, Y. Kusano, M. Takano, J. Phys. Soc. Jpn. 75 (2006) 104716.
[17] T.L. Chou, T.S. Chan, J.M. Chen, H. Yamauchi, M. Karppinen, J. Solid State Chem. 202 (2013) 27–32.
[18] M. Shizuya, M. Isobe, Y. Baba, T. Nagai, Y. Matsui, E. Takayama-Muromachi, J. Solid State Chem. 179 (2006) 3974–3980.
[19] M. Shizuya, M. Isobe, Y. Baba, T. Nagai, M. Osada, K. Kosuda, S. Takenouchi, Y. Matsui, E. Takayama-Muromachi, J. Solid State Chem. 180 (2007) 249–259.
[20] J. Pei, G. Chen, N. Zhou, J. Chem. Phys. 130 (2009) 044706.
[21] H. Yamauchi, M. Karppinen, Supercond. Sci. Technol 13 (2000) R33–R52.
[22] M. Shizuya, M. Isobe, E. Takayama-Muromachi, J. Appl. Phys. 102 (2007) 023704.
[23] M. Shizuya, M. Isobe, E. Takayama-Muromachi, Physica C 463–465 (2007) 178–181.
[24] S. Li, R. Funahashi, I. Matsubara, K. Ueno, S. Sodeoka, H. Yamada, J. Mater. Sci. Lett. 19 (2000) 1339–1341.
[25] K. Vidyasagar, J. Gopalakrishnan, C.N.R. Rao, Inorg, Chem. 23 (1984) 1206–1210.
[26] Y. Miyazaki, T. Miura, Y. Ono, T. Mashi, T. Goto, T. Kajitani, 21st International Conference on Thermoelectrics (ICT 02), (2002) pp. 226–229.
[27] W. Wong-Ng, G. Liu, J. Martin, E.L. Thomas, N. Lowhorn, J.A. Kaduk, J. Appl. Phys. 107 (2010) 033508.
[28] F. Delorme, C. Fernandez Martin, P. Marudhachalam, D. Ovono Ovono, G. Guzman, J. Alloys Compd. 509 (2011) 2311–2315.
[29] M. Isobe, M. Onoda, M. Shizuya, M. Tanaka, E. Takayama-Muromachi, J. Am. Chem. Soc. 129 (2007) 14585–14596.
[30] T. Klimczuk, H.W. Zandbergen, N.M. van der Pers, L. Viciu, V.L. Miller, M.H. Lee, R.J. Cava, Mater. Res. Bull. 41 (2006) 1673–1680.
[31] O. Haas, R.P.W.J. Struis, J.M. McBreen, J. Solid State Chem. 177 (2004) 1000–1010.
[32] M.K. Gupta, J. Phys. F: Met. Phys., Metal Phys 5 (1975) 359–362.
[33] B.T. Thole, G. van der Laan, Phys. Rev. B: Condens. Matter 38 (1988) 3158–3171.
[34] M.W. Ruckman, J. Chen, S.L. Qiu, P. Kuiper, M. Strongin, Phys. Rev. Lett. 67 (1991) 2533–2536.
[35] M. Imamura, N. Matsubayashi, H. Shimada, J. Phys. Chem. B 104 (2000) 7348–7353.
[36] C.D. Cappa, J.D. Smith, B.M. Messer, R.C. Cohen, R.J. Saykally, J. Phys. Chem. A 111 (2007) 4776–4785.
[37] J.B. MacNaughton, L. Näslund, T. Anniyev, H. Ogasawara, A. Nilsson, Phys. Chem. Chem. Phys. 12 (2010) 5712–5716.
[38] L. Karvonen, M. Valkeapää, R.S. Liu, J.M. Chen, H. Yamauchi, M. Karppinen, Chem. Mater. 22 (2010) 70–76.
[39] V.A.M. Brabers, Phys. Status Solidi 33 (1969) 563–572.
[40] A.L. Efros, B.I. Shklovskii, J. Phys. C: Solid State Phys. 8 (1975) L49.
[41] V.V. Rao, G. Rangarajan, R. Srinivasan, J. Phys. Chem. Solids 47 (1986) 395–400.